Dental Materials Journal 2013; 32(5): 725–733

Micromorphological cellular responses of MC3T3-E1 and RAW264.7 after exposure to water-dispersible silver nanoparticles stabilized by metal-carbon σ-bonds

Masanori HASHIMOTO[1], Hirokazu TOSHIMA[1], Tetsu YONEZAWA[2], Koji KAWAI[3], Takashi NARUSHIMA[2], Masayuki KAGA[1] and Kazuhiko ENDO[1]

[1] *Division of Biomaterials and Bioengineering, School of Dentistry, Health Sciences University of Hokkaido, 1757 Kanazawa, Ishikari-Tobetsu 061-0293, Japan*
[2] *Division of Materials Science and Engineering, Faculty of Engineering, Hokkaido University, Kita 13, Nishi 8, Kita-ku, Sapporo 061-0813, Japan*
[3] *Miyoshi Oil & Fat Co., Ltd., 4-66-1, Horikiri Katsushika-ku, 124-8510, Tokyo, Japan*
Corresponding author, Masanori HASHIMOTO; E-mail: has@hoku-iryo-u.ac.jp

With the continuous progress in nanomaterial development for biomedicine, the potential cytotoxicity of nanoparticles is drawing more attention and concern for clinical applications. The purpose of this study was to evaluate biological responses of new water-dispersible silver nanoparticles (Ag-NPs) stabilized by Ag-C σ-bonds in cultured murine macrophages (RAW264.7) and osteoblast-like cells (MC3T3-E1) using cell viability and morphological analyses. For RAW264.7, Ag-NPs seemed to induce cytotoxicity that was dependent on the Ag-NP concentration. However, no cytotoxic effects were observed in the MC3T3-E1 cell line. In microscopic analysis, Ag-NPs were taken up by MC3T3-E1 cells with only minor cell morphological changes, in contrast to RAW264.7 cells, in which particles aggregated in the cytoplasm and vesicles. The ability of endocytosis of macrophages may induce harmful effects due to expansion of cell vesicles compared to osteoblast-like cells with their lower uptake of Ag-NPs.

Keywords: Ag-NPs, Biocompatibility, Endocytosis, SEM, TEM

INTRODUCTION

Nanomaterials are increasingly used or tested in a wide variety of fields in materials and biological sciences owing to their unique size-dependent physicochemical properties. In particular, silver nanoparticles (Ag-NPs) have been intensively studied for applications as conductive materials[1,2] and catalysts[3,4]. In addition, the use of Ag-NPs is becoming more widespread in medicine and related applications owing to the strong antimicrobial activities of these materials[5-8], and other applications have been made possible by rapid developments in nanotechnology.

In most cases, metal NPs are stabilized by coordinative bonds between stabilizing groups and the particle surface to avoid aggregation. Commonly used stabilizing agents include various polymers such as PVP[1,9], and metal coordinating ligands of thiols[10] and amines[11]. Au-, Ti-, Pd- and Pt-NPs, which are stabilized by metal-carbon σ-bonds between surface metal atoms and aromatic ring moieties with long alkyl chains, can be prepared by reduction of the corresponding metal salts and the alkyl diazonium salt[12-14]. The chemical stability of metal-NPs is enhanced by the high bond strength of the σ-bond between the metal and carbon[13,14]. This is very significant to the synthesis of Ag-NPs stabilized by a Ag-C single bond because the Ag-S bond (bond strength 217 kJ mol^{-1}) is weak compared with the Au-S bond (bond strength 418 kJ mol^{-1})[15]. The novel characteristics of these stable metal NP materials has attracted growing interest in potential applications in diverse fields.

Our previous study showed the antimicrobial properties of our Ag-NPs with Ag-carbon σ-bonds against *Staphylococcus aureus*[16]. However, new properties of nanomaterials may also induce deleterious effects on living organs and cells, so the toxic potential of these materials must be methodically evaluated.

Therefore, the purpose of this study was to evaluate the effect of water-dispersible Ag-NPs stabilized by metal-carbon σ-bonds between surface metal atoms and aromatic ring moieties with hydrophilic groups on the cellular morphology and mitochondrial functions of macrophages (RAW264.7) and osteoblast-like cells (MC3T3-E1).

MATERIALS AND METHODS

Size distribution and UV-Vis measurement of Ag-NPs

Ag-NPs (supplied by Miyoshi Oil & Fat Co., Ltd., Tokyo, Japan) suspended in distilled water were used in this study. All procedures for synthesis of Ag-NPs were conducted according to previously reported methods[16]. A schematic illustration of the synthesized Ag-NPs is shown in Fig. 1. Prior to any tests, the solutions were sonicated for 30 s to reduce particle agglomeration. Transmission electron microscopy (TEM) samples were prepared for observation by evaporating a droplet of the aqueous dispersion of Ag-NPs onto a carbon-coated copper grid and observed using TEM at an accelerating voltage of 15 kV (Hitachi H-7100, Tokyo, Japan). Particle sizes were measured from enlarged images and their average size and distribution were calculated from these size data (n=300). A 500 μL aliquot of stock nanoparticles (100 μg/mL) was added to a cuvette, and the spectra were recorded between 350 nm and 650

Received Jul 31, 2012: Accepted Jun 12, 2013
doi:10.4012/dmj.2012-203 JOI JST.JSTAGE/dmj/2012-203

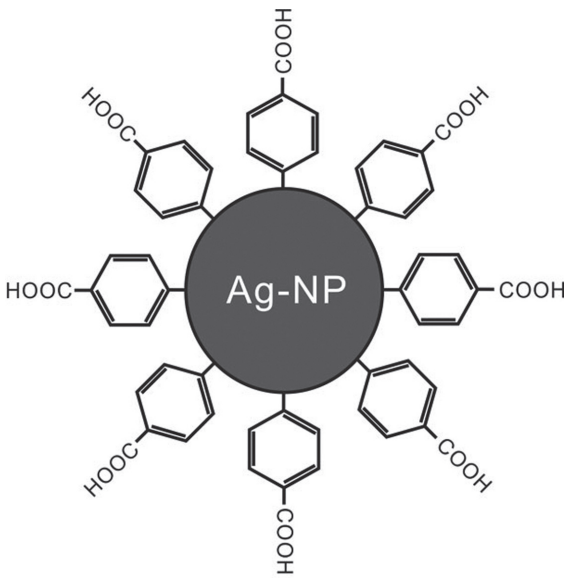

Fig. 1 Model structure of Ag-NPs used in this study.

nm using a UV-Vis spectrometer (Ultrospec 3100 *pro*, Amersham Pharmacia Biotech, Cambridge, UK). The scan speed was 750 nm/min, and the data interval was 1.0 nm. Milli-Q water was used as both the reference and blank for baseline subtraction.

Cell culture and preparation of conditioned medium

The RAW264.7 murine macrophage cell line (Riken Biosource Center Cell Bank, Tsukuba, Japan) were cultured at 37°C in α-minimal essential medium (Gibco, Grand Island, NY, USA) containing 10% (v/v) heat-inactivated fetal bovine serum (FBS), penicillin and streptomycin sulfate in a humidified atmosphere of 5% CO_2 in air. The MC3T3-E1 murine osteoblast cell line (Riken Biosource Center Cell Bank, Tsukuba, Japan) was maintained in Dulbecco's modified Eagle's medium (Sigma-Aldrich, Ayrshire, UK) with 10% FBS, media supplement (50 μg/mL L-ascorbic acid, 10 mmol/L glycerol phosphate disodium salt hydrate, and 50 nmol/L dexamethasone, Sigma-Aldrich, MO, USA) and antibiotics (penicillin and streptomycin sulfate). The osteogenic supplements are a well-documented formulation for inducing osteogenic differentiation of MC3T3-E1 cells and are used in combination with a cell viability assay[17,18]. The conditioned medium from this study was retained for future experiments to evaluate cytotoxicity and the mineralization properties of MC3T3-E1 using the results of this study. Cells were maintained in an incubator as described above.

Exposure of cells to Ag-NPs

Cells were seeded into Falcon 12-well plates (Corning, New York, USA) at a density of 5×10^4 cells per well in 1 mL of medium. Solutions of water-dispersible Ag-NPs were then immediately added to the cells at a total concentrations of 0 (control group), 0.5, 5, or 50 μg/mL (experimental groups). The Ag-NP-exposed cells were incubated for 24 h.

Table 1 Distribution of Ag-NP particle size

Particle size (nm)	0–10	10–20	20–30	30–40	≥40
Size distribution (%)	1.7	50.6	34.7	8.0	5.0

The average primary sizes of Ag-NPs were evaluated using TEM pictures, which showed spherical nanoparticles. The average particle size±standard deviation was 21.9±8.6 nm (n=300). Nanoparticles were examined in water and deposited onto Formvar/carbon-coated TEM grids.

Cell viability

Cell viability was measured using a WST-8 assay (CCK-8, Dojindo, Kumamoto, Japan). For the assay, water-soluble tetrazolium salt (WST-8) is reduced by dehydrogenase activities in the mitochondrial function of the cells to give a formazan dye. Cells in medium in 12-well plates (5×10^4 cells/1 mL medium/well) were incubated with and without Ag-NPs for 24 h. Subsequently, the medium was removed, and the cells were washed with twice with PBS. Then, 1 mL of medium and 100 μL of test solution of CCK-8 was added and the plate was incubated at 37°C for 1 h. After 1 h, the supernatant of the cells was placed in 96-well plates and the absorbance at 450 nm was measured on a microplate reader (Model 680, Bio-Rad, PA, USA).

Data were analyzed using one-way analysis of variance (ANOVA). When ANOVA showed significant differences between groups, Tukey's *post hoc* test was used to determine the specific pairs of groups between which statistically significant differences occurred. A p value of less than 0.05 was considered statistically significant (four independent repeats).

Micromorpholgical analysis of cells with internalized nanoparticles

The cells were optically observed and photographed with a phase-contrast inverted microscope (Eclipse TS100, Nikon, Tokyo, Japan) after 24 h incubation. For scanning electron microscopy (SEM) and TEM analyses, cells incubated with and without Ag-NPs were washed with PBS and fixed with 2.5% glutaraldehyde for 24 h. The cells were then post fixed in 1% osmium tetraoxide for 2 h, and washed and dehydrated in graded concentrations of ethanol (40, 50, 60, 70, 80, 90, and 100%) and hexamethyl disilazane (Wako Chemical). For SEM/energy-dispersive X-ray spectroscopy (EDX) analysis, the specimens were sputter-coated with gold or carbon and examined with SEM/EDX (SSX-550, Shimadzu, Kyoto, Japan) using an acceleration voltage of 15 kV in a vacuum. For TEM analysis, cells specimens were infiltrated and embedded in epoxy resin (EPON 812, TAAB, Berks, UK). Subsequently, ultrathin sections (90 μm) were cut with a diamond knife on a

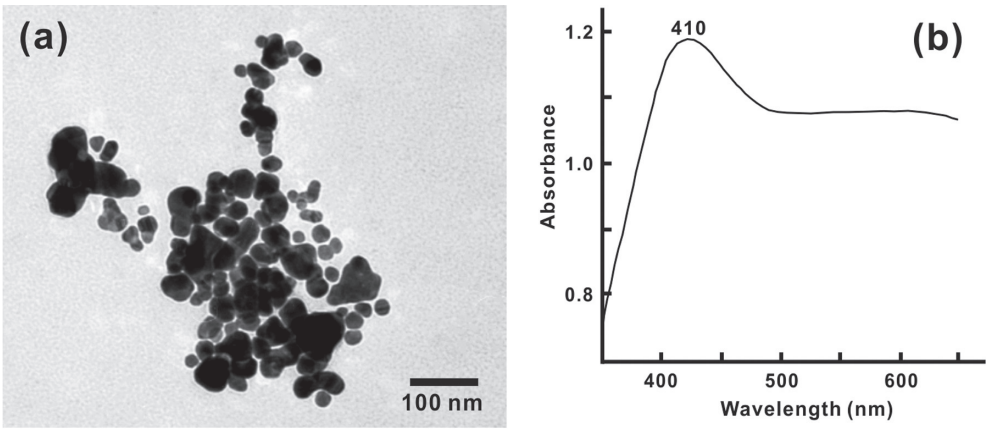

Fig. 2 TEM image (a) and UV-Vis absorbance (b) of Ag-NPs.
Characteristic plasmon absorption peaks were detected at 410 nm for Ag-NPs from the UV-Vis absorbance. The concentration of NPs was 100 μg/mL in the water dispersion.

microtome (Sorvall MT-5000, Du Pont, CA, USA). The sections were collected on copper grids, stained with saturated aqueous uranyl acetate, counter stained with 4% lead citrate, and observed using TEM (H-7100, Hitachi, Tokyo, Japan).

RESULTS

The TEM images were used to measure a mean diameter of 21.9 nm (Table 1).

Figure 2 shows a TEM image (a) and the UV-Vis absorbance (b) of Ag-NPs. Characteristic plasmon absorption peaks were detected at 410 nm, with the narrow peak of the UV-Vis absorbance indicating the nano-size of the Ag-NP particles. The absorption peaks also indicate that the nanoparticles are dispersible in water. The X-ray diffraction and X-ray photoelectron spectroscopy data characterizing these particles were described in our previous study[16].

Figure 3 shows the effects of Ag-NPs on cell viability in RAW264.7 and MC3T3-E1 cells.

For RAW264.7 cells, viability was significantly reduced after Ag-NP exposure ($p<0.05$). However, the viability of the three experimental groups of MC3T3-E1 cells was significantly greater than that of the control group ($p<0.05$).

Figure 4 shows inverted light microscopic images of RAW264.7 cells incubated with various concentrations of Ag-NPs (a: control, b: 5 μg/mL, c: 50 μg/mL) for 24 h. Following treatment with Ag-NPs, the number of vesicles in the plasma increased (Fig. 4b) compared with the control (Fig. 4a) and they appeared to be larger, with cytoplasmic agglomerated Ag-NPs (Fig. 4c). Cells incubated with 50 μg/mL of Ag-NPs/mL appeared to undergo the greatest change in morphology.

The light microscopic images in Fig. 5 show MC3T3-E1 cells incubated with two concentrations of Ag-NPs (a: 0.5 μg/mL, b: 50 μg/mL) for 24 h. The

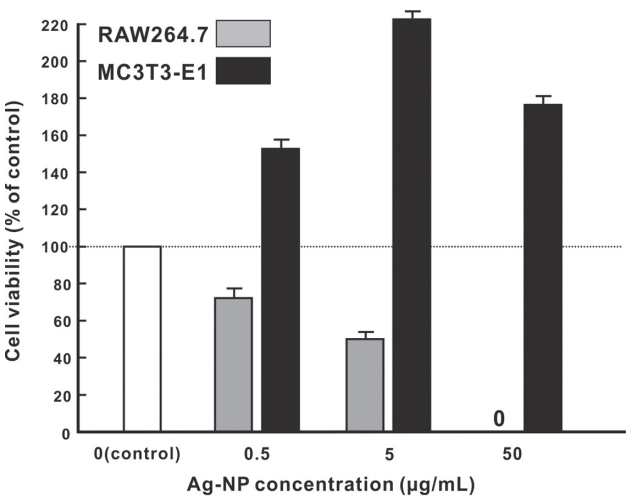

Fig. 3 Cell viability (WST-8 assay) of RAW264.7 and MC3T3-E1 cells cultured for 24 h in control medium (1 mL) and three other media containing 0.5, 5, or 50 μg/mL water-dispersible Ag-NPs.
Optical density values were calculated as percentages of that in the control group. Data are the mean±standard deviation of four independent repeats. Statistically significant differences were found among the four groups ($p<0.05$).

MC3T3-E1 cells display a spindle-like morphology on the surface, well spread in both experimental groups (Fig. 5a and b). Nanoparticles are observed in/upon cell surfaces (Fig. 5b) with few morphological changes compared with control cells (not shown). Although no clear appearance of nuclei were found in cells of the 0.5 μg/mL group at low magnification, dense Ag-NP deposition was found around nuclei in the 50 μg/mL group following Ag-NPs exposure (Fig. 5b).

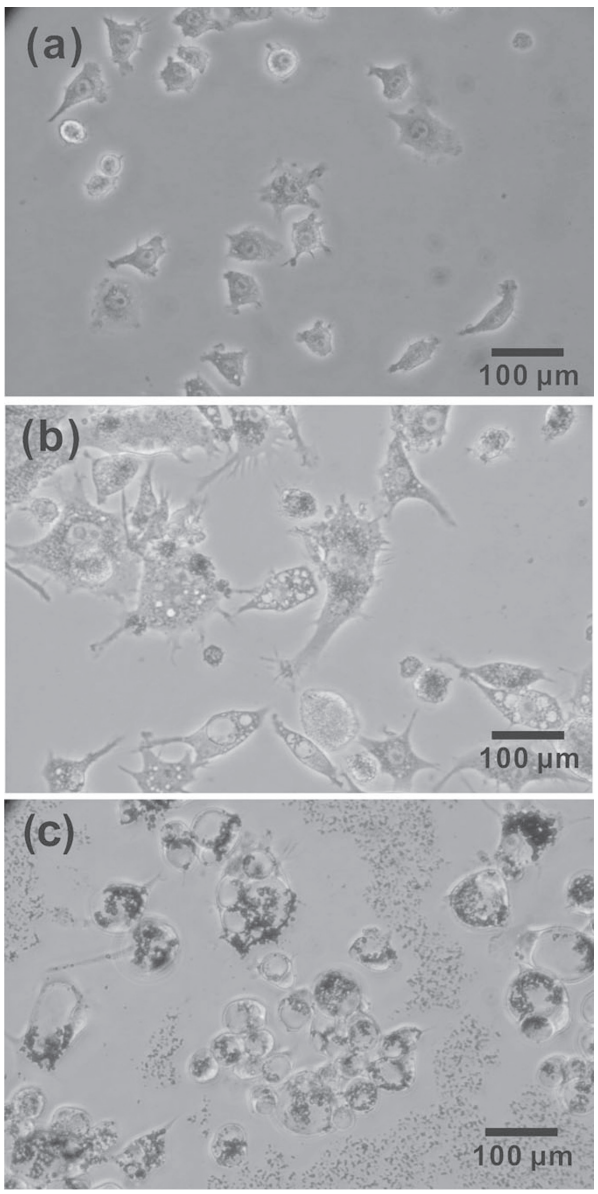

Fig. 4 Light microscopic images of RAW264.7 cells incubated with various concentrations of Ag-NPs (a: control, b: 5 μg/mL, c: 50 μg/mL).
The number and volume of lysosomes in cells exposed to Ag-NPs (b and c) were greater than those in the control cells (a).

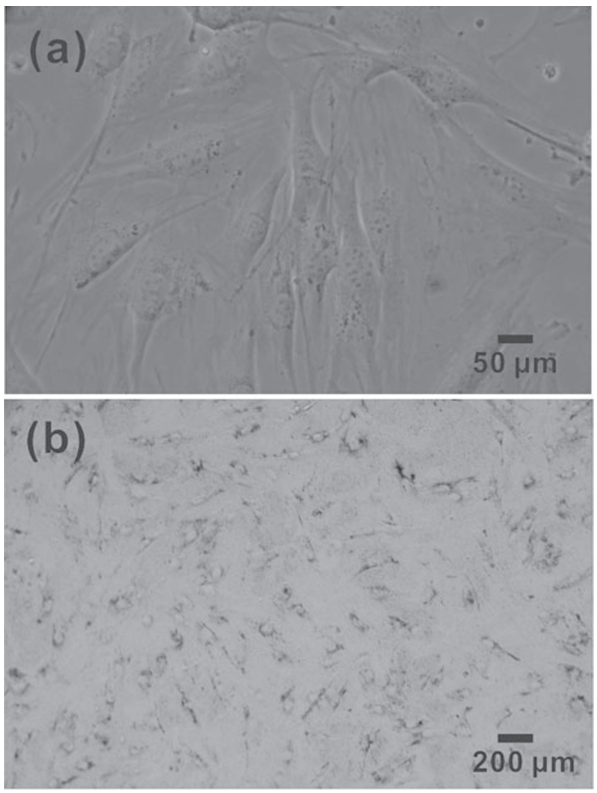

Fig. 5 Light microscopic images of MC3T3-E1 cells incubated with Ag-NPs (a: 0.5 μg/mL, b: 50 μg/mL). The extent of uptake of Ag-NPs was lower than that in RAW264.7 cells, and the formation of lysosomes was not clearly visible in MC3T3-E1 cells, unlike in RAW264.7 cells.

Figure 6 shows SEM/EDX images of RAW264.7 cells incubated with various concentrations of Ag-NPs (a and b: 50 μg/mL, c and d: 5 μg/mL). Particles and aggregates were observed in cell plasma by backscatter mode (Fig. 6b) and EDX (Fig. 6d). The distribution of Ag-NPs in and around the cells (RAW264.7 cells) was more clearly observed by backscatter mode compared with secondary electron mode as shown in Fig. 6a and b. The same results were obtained in the specimens of MC3T3-E1 cells or other different concentrations of Ag-NP exposure groups. Since the extents of deposition of Ag-NPs in cells were greatest in high concentrations of NP exposure (*i.e.* 50 μg/mL), the localization of Ag-NPs was clearly visible in the group of high concentrations NP exposure using backscatter mode of SEM and EDX analysis. By comparison with SEM electron modes (Fig. 6a and b), the Ag-NPs are readily distinguishable because of their uniform and characteristic size as electron dense contrast, which appears bright in backscatter electron mode. In backscatter mode images of Ag-NPs and cells, heavy elements (high atomic number of silver) are backscattered more strongly than light elements (low atomic number of cell or medium compositions), and thus appear brighter in an SEM image as shown in Fig. 6b. The EDX image demonstrates the Ag distribution of Ag-NPs (Fig. 6d) that were not detected in control specimens (not shown). The Ag-NP distribution in cells were clearly observed by EDX image (Fig. 6d), compared with secondary electron mode of SEM (Fig. 6c).

Figure 7 shows SEM/EDX images of MC3T3-E1 cells incubated with Ag-NPs (50 μg/mL). From the results

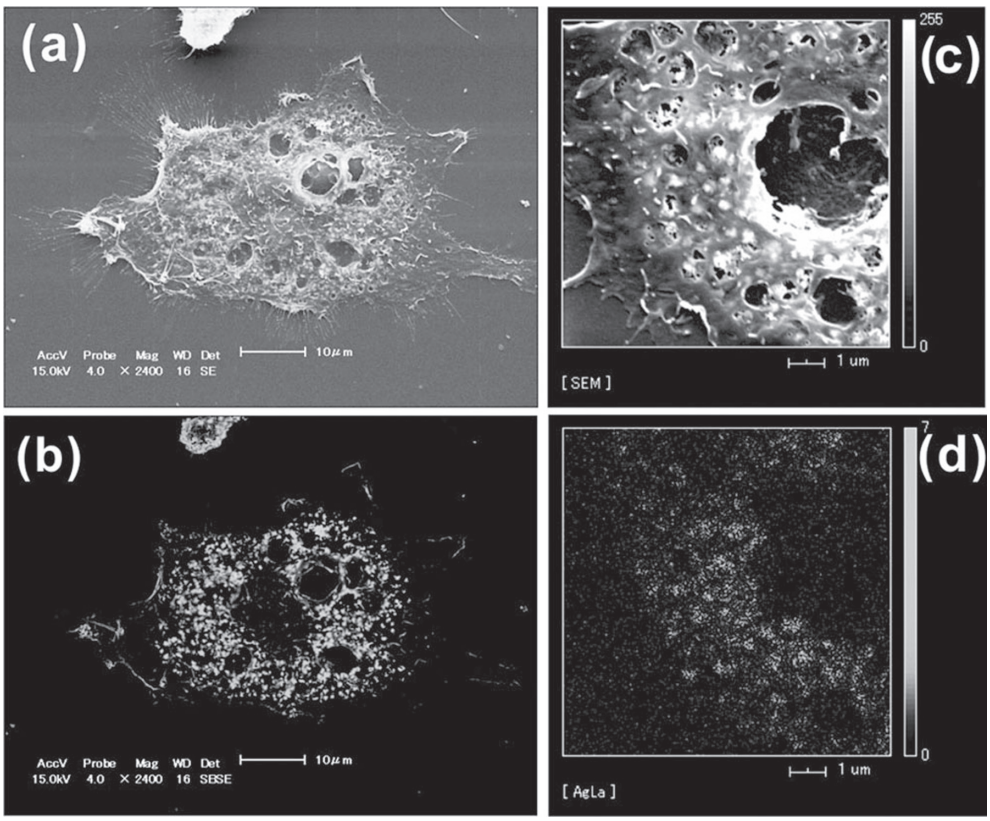

Fig. 6 SEM images of RAW264.7 presented using the secondary electron mode (a and c) and backscatter electron mode (b).
Cells were exposed to 50 μg/mL (a and b) and 5 μg/mL concentrations of Ag-NPs (c and d). Fig. 6b shows an SEM backscatter mode corresponding to the secondary electron mode image of Fig. 6a. Fig. 6d shows an EDX image corresponding to the SEM image of Fig. 6c.

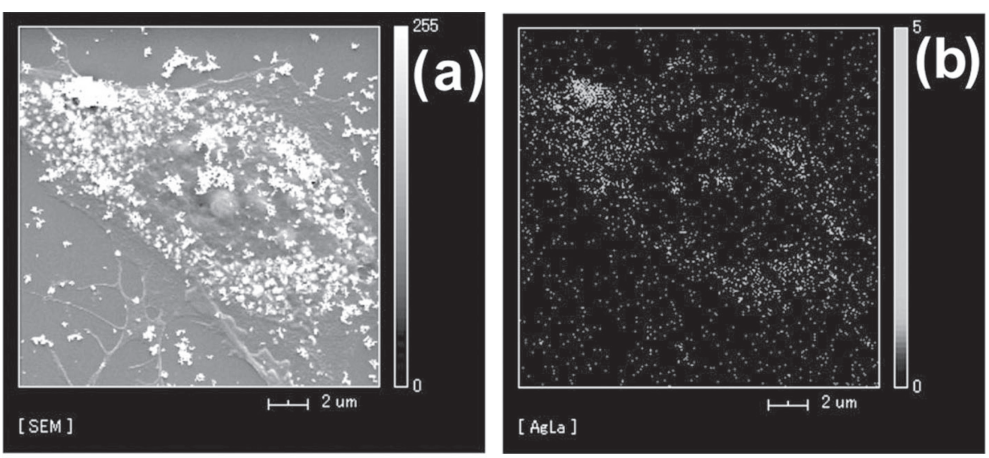

Fig. 7 SEM images of MC3T3-E1 cells presented using the secondary electron mode (a: 50 μg/mL Ag-NPs).
Fig. 7b shows an EDX image corresponding to the SEM image of Fig. 7a. The silver particles are not clearly visible inside these cells, in contrast to SEM images of RAW264.7 cells (Fig. 6).

obtained by SEM in many cases of MC3T3-E1 cells, it was difficult to determine clearly whether the Ag-NPs were localized in or upon cells. However, in the case of Fig. 7, the Ag accumulation could be identified by EDX (Fig. 7b), and the localization of particles upon cells can be partially identified by an SEM image (Fig. 7a).

Figure 8 shows TEM images of RAW264.7 cells incubated with Ag-NPs (a: control, b and d: 50 μg/mL, c: 5 μg/mL) for 24 h. Nuclei or cell plasma projections are clearly visible in TEM images of the control group (Fig. 8a). Enlarged vesicles with large agglomerates of Ag-NPs are evident in cells incubated with 50 μg Ag-NPs (Fig. 8b). Most particles were internalized, and localized to the vesicles or cytoplasm but not the nucleus (Fig. 8c). Figure 8d shows necrosis of cells with rupture of the cell membrane.

Figure 9 shows TEM images of MC3T3-E1 with 50 μg/mL Ag-NP. Internalization of Ag-NPs is visible in the cytoplasm and vesicles. The number of particles taken up by MC3T3-E1 cells was lower than that for RAW264.7. Particles were not observed in the nucleus. In Fig. 9b, many particles were located upon the cell surfaces that were similar morphological phase of SEM picture of Fig. 7a. Although internalization of Ag-NPs is visible in the vesicles (Fig. 9a), no morphological changes were found in cells and organelles of MC3T3-E1 cells such as the expansion of vesicles and cell volume that were found in RAW264.7 cells. Any increase in the number and volume of vesicles in MC3T3-E1 cells was minor, compared with RAW264.7 cells. Projection of the cell membrane for particle uptake can be seen in Fig. 9b and c.

DISCUSSION

With the advancement of nanotechnology, new Ag-NPs have been synthesized and shown to have antimicrobial properties, making them attractive for potential dental and medical use if they possess biocompatibility for cells or organs[19]. Recent studies have shown quaternary ammonium dimethacrylate and Ag-NPs to be effective as primers for dental adhesives because of their antibacterial properties and bond strength[8,20]. The main purpose of surface modification of Ag-NPs (*e.g.*

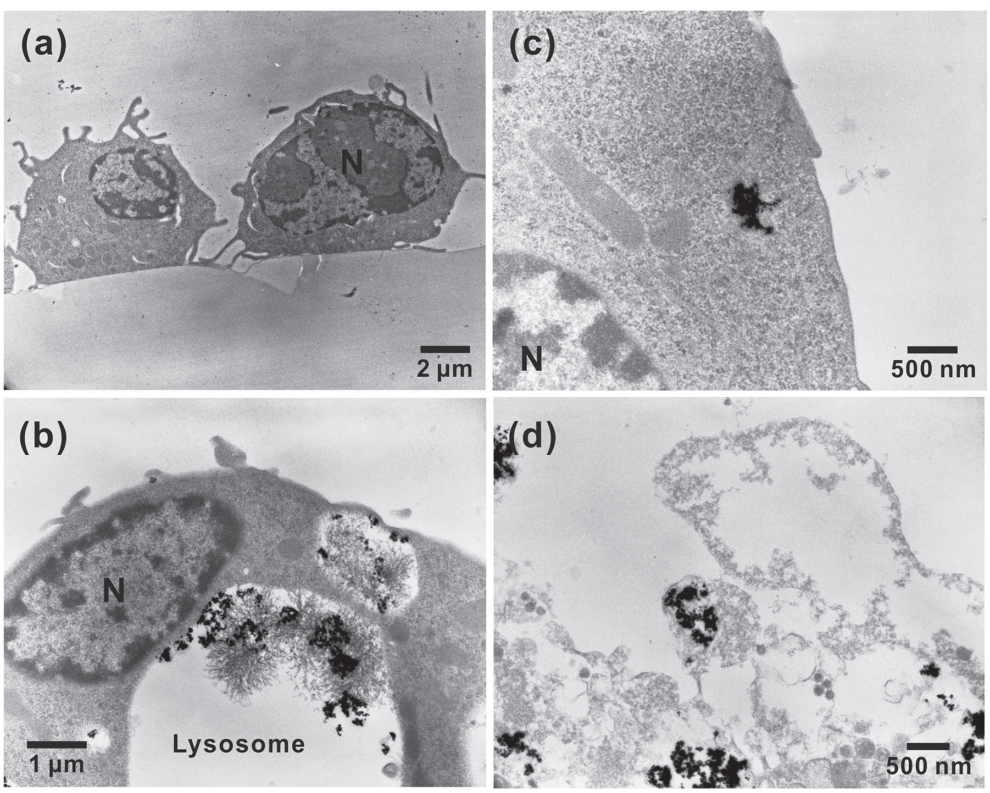

Fig. 8 TEM micrographs of RAW264.7 cells (macrophages) incubated with various concentrations of Ag-NPs (a: control, b and d: 50 μg/mL, c: 5 μg/mL). Nanoparticles appear to be localized in the cytoplasm (c) and excluded from the nuclei. The nanoparticles tend to be agglomerated in micron-sized clusters inside the cells, making the lysosomes larger (b) than in the control condition (a). The plasma membrane is ruptured, allowing leakage of organelles and cytoplasm into the intercellular space (d). N: nucleus

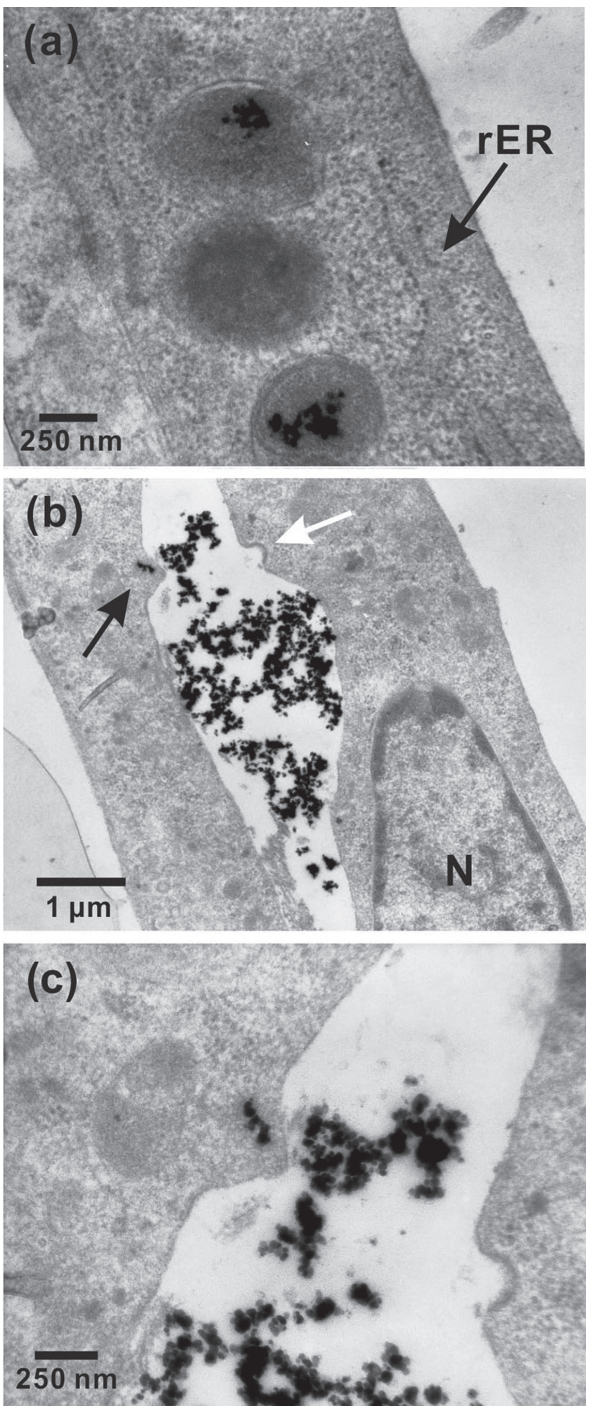

Fig. 9 TEM micrographs of MC3T3-E1 cells incubated with a solution of 50 μg/mL Ag-NPs.
Localization of the particles to lysosomes is shown in Fig. 9a. Two different stages of the cellular uptake process are observed in Figs. 9b and 9c. A projection from the plasma membrane surface (white arrow) and wrapping of the particles for uptake (black arrow) can be seen in Fig. 9b. A higher magnification view of Fig. 9b is shown in Fig. 9c. Particle uptake into MC3T3-E1 cells was less than in RAW264.7 cells. N: nucleus, rER: rough-surfaced endoplasmic reticulum.

with hydrophobic/hydrophilic coatings) is to obtain water-dispersive properties. It has also been reported that Ag-NPs dissolve and generate silver ions, resulting in disruption of ATP production, DNA replication, and ROS generation under certain cellular condition[19,21]. Surface capping of nanoparticles prevented silver ion release, leading to decreased cytotoxicity for cells and organs[22,23]. Therefore, this modification can enhance stability and improve the biocompatibility of these materials[19].

Our results for cell viability showed that Ag-NPs had cytotoxic effects on RAW264.7 cells, especially at higher concentrations. However, the viability of MC3T3-E1 cells was unexpectedly increased after Ag-NP exposure.

Recent studies have reported conflicting data regarding the cytotoxicity of Ag-NPs in cells. Studies using various cell lines reported that Ag-NPs affected mitochondrial function and induced cell necrosis or apoptosis[24,25]. However, other investigators found no such cytotoxic effects of Ag-NPs on living cells[26]. In addition, weakened or absent cell responses have been reported with other nanoparticles such as Au-NPs[27] and nanodiamonds[28], suggesting that the cytotoxicity is affected by the physicochemical characteristics of the particles (*e.g.* their size, size distribution, shape, state of dispersion, physical and chemical properties, surface area and porosity, surface chemistry) and by cell characteristics (*e.g.* cell line, number of cells per well, and the period of culture before and/or after exposure to nanoparticles)[17,24-26,29,30]. A recent study showed a decrease in MC3T3-E1 cell viability after exposure to Ag-NPs using the WST-8 assay[31], but this study used different test conditions for cell culture and exposure to Ag-NPs, which may explain the disparity between their results and ours.

The localization of Ag-NPs, whether in the cytoplasm or lysosomes, was not clearly visible because vesicles tended to collapse under the high vacuum used to observe the specimens, resulting in nano-sized artifacts in the SEM analysis. The localization and aggregation of particles in the lysosomes of RAW264.7 cells was visible by light microscopy and clearly observed by TEM. The number of Ag-NPs observed in plasma was lower than in lysosomes. Particle aggregation in lysosomes was observed in many RAW264.7 cells, and these lysosomes may have been enlarged like a balloon owing to release of hydrolase enzymes (*e.g.* glycosidase, lipase, phosphatase, nuclease). The intracellular vesicles are smaller and less numerous in the control and low concentration (0.5 μg/mL) groups, compared with those in cells incubated with the higher concentration of Ag-NPs (50 μg/mL). Although the lysosome size varies from 0.1–1.2 μm, the RAW264.7 cells of the control groups were enlarged by Ag-NP exposure. We hypothesize that the enlarged volume of balloon-like vesicles may induce malfunction of other organelles in the cytoplasm and, finally, explode the cell membrane, leading to cell death as shown in Fig. 8d. To our knowledge, no TEM report has been available on the functional disorder of lysosomes of RAW264.7

macrophages demonstrated in the present study.

Another interesting finding was that there were no (or only minor) changes in the number and volume of lysosomes in MC3T3-E1 cells. Moreover, the uptake of Ag-NPs into vesicles or the cytoplasm of MC3T3-E1 cells was less apparent than in macrophages. Judging from our findings, the uptake of Ag-NPs may play only a limited role in cytotoxicity for MC3T3-E1 cells because we observed minimal toxicity in our viability assays (Fig. 3), in stark contrast with our results for RAW264.7. Figure 9 shows two different MC3T3-E1 cells. A plasma membrane projection is visible in one cell, and the opposite side of the cell engulfs a particle aggregate after internalization. These images provide evidence of the early endocytosis process of MC3T3-E1 cells. Mustafa *et al.*[27] have shown that, for MC3T3-cells, large agglomerates of NPs on the cell surfaces are rapidly internalized into cells by endocytosis after exposure to a high concentration of Au-NPs. In contrast, a single particle may individually penetrate a cell by diffusion *via* a cell membrane pore at a lower concentration of Ag-NPs. Since the Ag-NP uptake by endocytosis was greater than that by diffusion for both RAW264.7 and MC3T3-E1, because of the particle size in the cells (aggregation state), the endocytic process of nanoparticles may be the main pathway of the particles. Although endocytosis is not a typical characteristic of osteoblast-like cells, the uptake of bacteria was observed in MC3T3-E1 cells during mycobacterial infection[32].

Endocytosis is a basic cellular process and proceeds by one or more of three different mechanisms: pinocytosis, phagocytosis, and receptor-mediated endocytosis. Phagocytosis and pinocytosis are distinguished by the particle size or vesicles. When uptake of NPs occurs *via* receptor-mediated endocytosis, the trapped particles coat the cell near the membrane inside the vesicle[26]. However, the trapped particles would lead to aggregation in the vesicle in the case of simple pinocytosis or endocytosis[26]. Based on these previous results, we conclude that the Ag-NP uptake in the present study is morphologically most like endocytosis, suggesting that this is the main mechanism of uptake.

Hackenberg *et al.*[33] have shown, using TEM, that Ag-NPs translocate into the nuclei of human mesenchymal stem cells. Another TEM study showed the presence of Ag-NPs in nuclei and nucleoli of human lung fibroblasts and human glioblastoma cells[34]. Damage to DNA may arise from binding of particles or oxidative damage. The nuclear deposition of Ag-NPs would be expected to have lethal effects on DNA synthesis, chromosomal morphology and segregation, affecting the DNA and cell division. Mahmood *et al.*[35] reported abnormal cellular morphology in cells after exposure to Ag-NPs with a high concentration of an apoptotic agent. This morphology was characterized microscopically by nuclear chromatin condensation, cellular membrane blebbing, cellular shrinkage, cellular lysis and disintegration. Cellular uptake of nanoparticles depends on their size being within the range of 15–100 nm. For nuclear deposition of metal nanoparticles in particular, the particle size is thought to be correlated with their ability to diffuse into the nucleus[36]. We speculate that Ag-NPs with a diameter of 21.9 nm cannot enter the nucleus owing to a 9 nm pore size exclusion limit for passive diffusion across the nuclear membrane[36,37]. Although no apparent Ag-NP penetration was observed in the nuclear region in the cells tested, it is possible that similar morphological nuclear changes may occur under different test conditions using the same Ag-NPs.

CONCLUSIONS

We conclude that the cytotoxic effects and morphological cellular changes in response to Ag-NPs appear to be cell-specific. The toxicities of nano-particles depend on the stability of the core composition. Toxic metals have the potential to leach when the chemical structure is changed in biological systems, but this effect can be minimized when the σ-bond between the metal and carbon is strong. Thus, the stability and dispersion characteristics are special and important properties of a nanoparticle material, and could be used to prevent or reduce the leaching of the silver core under biological circumstances. However, lysosome dysfunction induced by Ag-NPs in RAW264.7 cells shows the need for further optimization of particle composition.

ACKNOWLEDGMENTS

This work was partially supported, in part, by Grants-in-Aid for Scientific Research (C) (No. 23592894) from Japan Society for the Promotion of Science (JSPS).

REFERENCES

1) Wiley B, Sun Y, Xia Y. Synthesis of silver nanostructures with controlled shapes and properties. Acc Chem Res 2007; 40: 1067-1076.
2) Chen D, Qiao X, Qiu X, Chen J. Synthesis and electrical properties of uniform silver nanoparticles for electronic applications. J Mater Sci 2009; 44: 1076-1081.
3) Zhaoa H, Zhoua J, Luoa H, Zenga C, Lia D, Liu Y. Synthesis, characterization of Ag/MCM-41 and the catalytic performance for liquid-phase oxidation of cyclohexane. Catal Lett 2006; 108: 49-54.
4) Chen Y, Wang C, Liu H, Qiu J, Bao X. Ag/SiO_2: a novel catalyst with high activity and selectivity for hydrogenation of chloronitrobenzenes. Chem Commun 2005; 14: 5298-5300.
5) Kong H, Jang J. Antibacterial properties of novel poly(methyl methacrylate) nanofiber containing silver nanoparticles. Langmuir 2008; 24: 2051-2056.
6) Sanpui P, Chattopadhyay A, Ghosh SS. Induction of apoptosis in cancer cells at low silver nanoparticle concentrations using chitosan nanocarrier. Appl Mater Interfaces 2011; 3: 218-228.
7) Chen X, Schluesener HJ. Nanosilver: A nanoproduct in medical application. Toxicol Lett 2008; 176: 1-12.
8) Cheng L, Zhang K, Melo MAS, Weir MD, Zhou X, Xu HHK. Anti-biofilm dentin primer with quaternary ammonium and silver nanoparticles. J Dent Res 2012; 91: 598-604.
9) Li Z, Gu A, Guan M, Zhou Q, Shang T. Large-scale synthesis of silver nanowires and platinum nanotubes. Colloids Polym Sci 2010; 288: 1185-1191.
10) Rao TUB, Pradeep T. Luminescent Ag7 and Ag8 clusters by

interfacial synthesis, angew. Angew Chem Int Ed Engl 2010; 49: 3925-3929.
11) Mishra T, Sahu RK, Lim S-H, Salamanca-Riba LG, Bhattacharjee S. Hexadecylamine capped silver and gold nanoparticles: Comparative study on formation and self-organization. Mater Chem Phys 2010; 123: 540-545.
12) Mirkhalaf F, Paprotny J, Schiffrin DJ. Synthesis of metal nanoparticles stabilized by metal-carbon bonds. J Am Chem Soc 2006; 128: 7400-7401.
13) Ghosh D, Pradhan S, Chen W, Chen S. Titanium nanoparticles stabilized by Ti-C covalent bonds. Chem Mater 2008; 20: 1248-1250.
14) Ghosh D, Chen S. Palladium nanoparticles passivated by metal-carbon covalent linkages. J Mater Chem 2008; 18: 755-762.
15) Haynes WM. CRC handbook of chemistry and physics: a ready-reference book of chemical and physical data. CRC Press, Boca Raton, FL, 2010.
16) Kawai K, Narushima T, Kaneko K, Kawakami H, Matsumoto M, Hyono A, Nishihara H, Yonezawa T. Synthesis and antibacterial properties of water-dispersible silver nanoparticles stabilized by metal-carbon σ-bonds. Appl Surf Sci 2012; 262: 76-80.
17) Taira M, Nakao H, Takahashi J, Araki Y. Effects of two vitamins, two growth factors and dexamethasone on the proliferation of rat bone marrow stromal cells and osteoblastic MC3T3-E1 cells. J Oral Rehabil 2003; 30: 697-701.
18) Yasuda Y, Tatematsu Y, Fujii S, Maeda H, Akamine A, Torabinejad M, Saito T. Effect of MTAD on the differentiation of osteoblast-like cells. J Endod 2010; 36: 260-263.
19) Marambio-Jones C, Hoek EMV. A review of the antibacterial effects of silver nanomaterials and potential implications for human health and the environment. J Nanopart Res 2010; 12: 1531-1551.
20) Cheng L, Weir MD, Xu HHK, Antonucci JM, Kraigsley AM, Lin NJ, Zhou X. Antibacterial amorphous phosphate nanocomposites with a quaternary ammonium dimethacrylate and silver nanoparticles. Dent Mater 2012; 28: 561-572.
21) Asharani PV, Mun GLK, Hande MP, Valiyaveettil S. Cytotoxicity and genotoxicity of silver nanoparticles in human cells. ACS Nano 2009; 2: 279-290.
22) Smetana AB, Klabunde KJ, Marchin GR, Sorensen CM. Biocidal activity of nanocrystalline silver powders and particles. Langmuir 2008; 24: 7457-7464.
23) Choi O, Clevenger TE, Deng B, Surampalli RY, Ross L Jr, Hu Z. Role of sulfide and ligand strength in controlling nanosilver toxicity. Water Res 2009; 43: 1879-1886.
24) Nishanth RP, Jyotsna RG, Schlager JJ, Hussain SM, Reddanna P. Inflammatory responses of RAW 264.7 macrophages upon exposure to nanoparticles: Role of ROS-NFκB signaling pathway. Nanotoxicology 2011; 5: 502-516.
25) Park J, Lim DH, Lim HJ, Kwon T, Choi JS, Jeong S, Choi IH, Cheon J. Size dependent macrophage responses and toxicological effects of Ag nanoparticles. Chem Commun 2011; 47: 4382-4384.
26) Yen HJ, Hsu SH, Tsai CL. Cytotoxicity and immunological response of gold and silver nanoparticles of different sizes. Small 2009; 13: 1553-1561.
27) Mustafa T, Watanabe F, Monroe W, Mahmood M, Xu Y, Saeed LM, Karmakar A, Casciano D, Ali S, Biris AS. Impact of gold nanoparticles concentration on their cellular uptake by MC3T3-E1 mouse osteoblastic cells as analyzed by transmission electron microscopy. J Nanomedic Nanotechnol 2011; 2: 61.
28) Schrand AM, Huang H, Carlson C, Schlager JJ, Ōsawa E, Hussain SM, Dai L. Are diamond nanoparticles cytotoxic? J Phys Chem B 2007; 111: 2-7.
29) Park MVDZ, Neigh AM, Vermeulen JP, de la Fonteyne LJJ, Verharen HW, Briedé JJ, van Loveren H, de Jong WH. The effect of particle size on the cytotoxicity, inflammation, developmental toxicity and genotoxicity of silver nanoparticles. Biomaterials 2011; 32: 9810-9817.
30) Powers KW, Brown SC, Krishna VB, Wasdo SC, Moudgil BM, Roberts SM. Research strategies for safety evaluation of nanomaterials. Part VI. Characterization of nanoscale particles for toxicological evaluation. Toxicol Sci 2006; 90: 296-303.
31) Kim TH, Park HS, Shin US, Gong MS, Kim HW. Size-dependent cellular toxicity of silver nanoparticles. J Biomed Mater Res 2012; 100: 1033-1043.
32) Hotokezawa H, Kitamura A, Matsumoto S, Hanazawa S, Amano S, Yamada T. Internalization of *Micobacterium bovis* Bacillus Camette-Guérin into osteoblast-like MC3T3-E1 cells and bone resorptive responses of the cells against the infection. Scand J Immunol 1998; 47: 453-458.
33) Hackenberg S, Scherzed A, Kessler M, Hummel S, Technau A, Froelich K, Ginzkey C, Koehler C, Hagen R, Kleinsasser N. Silver nanoparticles: Evaluation of DNA damage, toxicity and functional impairment in human mesenchymal stem cells. Toxicol Lett 2011; 201: 27-33.
34) AshaRani PV, Hande MP, Valiyaveettil S. Anti-proliferative activity of silver nanoparticles. BMC Cell Biol 2009; 10: 65.
35) Mahmood M, Casciano DA, Mocan T, Iancu C, Xu Y, Mocan L, Iancu DT, Dervishi E, Li Z, Abdalmuhsen M, Biris AR, Ali N, Howard P, Biris AS. Cytotoxicity and biological effects of functional nanomaterials delivered to various cell limes. J Appl Toxicol 2009; 30: 74-83.
36) Paine PL, Moore LC, Horowitz SB. Nuclear-envelope permeability. Nature 1975; 254: 109-114.
37) Gu YJ, Cheng J, Lin CC, Lam YW, Cheng SH, Wong WT. Nuclear penetration of surface functionalized gold nanoparticles. Toxicol Appl Pharmacol 2009; 237: 196-204.